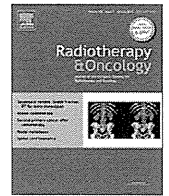


neck squamous cell carcinoma with a limited field of postoperative radiotherapy. Jpn J Clin Oncol 43:719-725,2013

9) Kawashima M, Arijji T, Kameoka S, Ueda T, Kohno R, Nishio T, Arahira S, Motegi A, Zenda S, Akimoto T, Tahara M, Hayashi R. Locoregional control after intensity-modulated radiotherapy for nasopharyngeal carcinoma with an anatomy-based target definition. Jpn J Clin Oncol 43: 1218-1225, 2013

10) Yasuda K, Onimaru R, Okamoto S, Shiga T, Katoh N, Tsuchiya K, Suzuki R, Takeuchi W, Kuge Y, Tamaki N, Shirato H. [18F]fluoromisonidazole and a new PET system with semiconductor detectors and a depth of interaction system for intensity modulated radiation therapy for nasopharyngeal cancer. Int J Radiat Oncol Biol Phys. 85:142-7, 2013



## Head and neck cancer

## Volume and dosimetric changes and initial clinical experience of a two-step adaptive intensity modulated radiation therapy (IMRT) scheme for head and neck cancer

Tamaki Nishi<sup>a,b,\*</sup>, Yasumasa Nishimura<sup>a</sup>, Toru Shibata<sup>a</sup>, Masaya Tamura<sup>a</sup>, Naohiro Nishigaito<sup>b</sup>, Masahiko Okumura<sup>b</sup>

<sup>a</sup> Department of Radiation Oncology, Kinki University Faculty of Medicine, Osaka-Sayama, Japan; <sup>b</sup> Department of Central Radiological Service, Kinki University Faculty of Medicine, Osaka-Sayama, Japan

## ARTICLE INFO

## Article history:

Received 23 May 2012

Received in revised form 12 November 2012

Accepted 18 November 2012

Available online 19 January 2013

## Keywords:

Adaptive radiation therapy

Intensity modulated radiation therapy

Head and neck cancer

## ABSTRACT

**Purpose:** The aim of this study was to show the benefit of a two-step intensity modulated radiotherapy (IMRT) method by examining geometric and dosimetric changes.

**Material and Methods:** Twenty patients with pharyngeal cancers treated with two-step IMRT combined with chemotherapy were included. Treatment-planning CT was done twice before IMRT (CT-1) and at the third or fourth week of IMRT for boost IMRT (CT-2). Transferred plans recalculated initial plan on CT-2 were compared with the initial plans on CT-1. Dose parameters were calculated for a total dose of 70 Gy for each plan.

**Results:** The volumes of primary tumors and parotid glands on CT-2 regressed significantly. Parotid glands shifted medially an average of 4.2 mm on CT-2. The mean doses of the parotid glands in the initial and transferred plans were 25.2 Gy and 30.5 Gy, respectively. D<sub>2</sub> (dose to 2% of the volume) doses of the spinal cord were 37.1 Gy and 39.2 Gy per 70 Gy, respectively. Of 15 patients in whom xerostomia scores could be evaluated 1–2 years after IMRT, no patient complained of grade 2 or more xerostomia.

**Conclusions:** This two-step IMRT method as an adaptive RT scheme could adapt to changes in body contour, target volumes and risk organs during IMRT.

© 2012 Elsevier Ireland Ltd. All rights reserved. Radiotherapy and Oncology 106 (2013) 85–89

A significant advance in radiation therapy (RT) is the successful clinical use of intensity modulated radiation therapy (IMRT). IMRT is effective, especially for head and neck cancers, since the clinical target volumes (CTV) are in contiguity with organs at risk such as the salivary glands, brain stem, and spinal cord. Two randomized clinical trials comparing IMRT and conventional RT for patients with early-stage nasopharyngeal cancer (NPC) showed a significant benefit of IMRT on salivary function and quality of life (QOL) of patients [1,2].

Although it is very encouraging to use this new technique to improve the therapeutic ratio, questions remain as to whether the conformation of target coverage and normal tissue sparing may cause marginal failure [3]. As treatment planning and quality assurance (QA) of IMRT plans require a long time to prepare, most investigators use the initial IMRT plan for the whole course of IMRT. However, significant anatomic changes, including shrinking of the primary tumor or nodal masses and body weight loss during fractionated RT, have been reported for head and neck cancers [4,5]. Our previous analysis revealed that the volume of the parotid glands decreased to 74% of

the initial volume during the course of IMRT [6]. These changes in body contour, target volumes and risk organs during IMRT can affect the dose distribution to the target volume and risk organs, which can be a cause of marginal recurrence or late toxicities. In fact, marginal recurrences after IMRT for head and neck cancer have been reported by several investigators [7,8].

To avoid the risk of changes in the dose distribution during IMRT of 7–8 weeks, we adopted a two-step IMRT method for head and neck cancers. For all patients, treatment-planning computed tomography (CT) was done before IMRT (CT-1) and at the third or fourth week of IMRT for the treatment planning of boost IMRT after 46–50 Gy (CT-2) [6,7]. The aim of this study was to show the benefit of our adaptive RT scheme using a two-step IMRT method by examining the geometric and dosimetric changes in patients with head and neck cancer.

## Materials and methods

## Patients' characteristics and treatment methods

Between February 2006 and April 2010, 20 consecutive patients with pharyngeal cancers treated by a two-step IMRT method combined with concurrent chemotherapy were analyzed. Patients and

\* Corresponding author. Address: Department of Central Radiological Service, Kinki University Faculty of Medicine, 377-2, Ohno-Higashi, Osaka-Sayama, Osaka 589-8511, Japan.

E-mail address: [tamakinishi\\_1213@kxa.biglobe.ne.jp](mailto:tamakinishi_1213@kxa.biglobe.ne.jp) (T. Nishi).

**Table 1**  
Study cohort and treatment characteristics, and their clinical results.

Case	Primary site	T stage	N stage	UICC stage	Total(Boost) RT dose	Concurrent chemotherapy	Neck dissection	Parotid D <sub>mean</sub> (sum)	Xerostomia at 1–2 year	Overall survival	Local control
1	HPC	T1	N2b	VI A	70(20)Gy	Cisplatin	Y	25.6	–	15 m DOD	15 m LC
2	HPC	T2	N2b	VI A	70(20)Gy	Cisplatin	Y	21.6	Grade 0	22 m DOD	9 m rec
3	HPC	T1	N2a	VI A	70(20)Gy	S-1	N	22.5	–	9 m DID	9 m LC
4	HPC	T2	N3	VI B	70(20)Gy	Cisplatin	Y	21.6	Grade 0	56 m NED	56 m LC
5	OPC	T3	N2b	VI A	70(20)Gy	Cisplatin	N	26.8	Grade 1	53 m DOD	46 m rec
6	OPC	T2	N2	VI A	60(20)Gy	Cisplatin, 5FU	Y	29.0	–	17 m DOD	6 m rec
7	OPC	T1	N2b	VI A	66(16)Gy	Cisplatin	Y	25.1	Grade 0	53 m NED	53 m LC
8	OPC	T4a	N0	VI A	70(20)Gy	Cisplatin	N	17.5	Grade 1	36 m NED	36 m LC
9	OPC	T2	N2C	VI A	66(16)Gy	CBDCA	N	24.5	–	9 m DOD	6 m rec
10	OPC	T4a	N0	VI A	70(20)Gy	Cisplatin	N	21.7	–	8 m DOD	6 m rec
11	NPC	T3	N0	III	70(20)Gy	Cisplatin	N	23.0	Grade 0	78 m NED	78 m LC
12	NPC	T2b	N1	II	70(20)Gy	Cisplatin	N	24.9	Grade 0	74 m NED	74 m LC
13	NPC	T2b	N1	II	70(20)Gy	Cisplatin	N	27.8	Grade 0	73 m NED	73 m LC
14	NPC	T3	N0	III	70(20)Gy	Cisplatin	N	23.9	Grade 0	73 m NED	73 m LC
15	NPC	T1	N0	I	70(20)Gy	Cisplatin	N	22.4	Grade 0	70 m NED	70 m LC
16	NPC	T1	N1	II	70(20)Gy	Cisplatin	N	24.8	Grade 0	68 m NED	68 m LC
17	NPC	T3	N1	III	70(20)Gy	Cisplatin	N	23.9	Grade 0	68 m NED	68 m LC
18	NPC	T3	N2	III	70(20)Gy	Cisplatin	N	23.6	Grade 0	65 m NED	65 m LC
19	NPC	T1	N2	III	70(20)Gy	Cisplatin	Y	21.4	Grade 1	59 m NED	59 m LC
20	NPC	T3	N2	III	68(20)Gy	Cisplatin	N	26.2	Grade 0	57 m NED	57 m LC

Abbreviations: HPC, hypopharyngeal cancer; OPC, oropharyngeal cancer; NPC, nasopharyngeal cancer; CBDCA, carboplatin; y, yes; n, no; m, months; NED, no evidence of the disease; DOD, died of the disease; DID, died of the intercurrent disease; LC, loco-regional control.

tumor characteristics and their clinical results are shown in Table 1. All patients were treated with whole neck IMRT to 46–50 Gy/23–25 fractions, followed by boost IMRT limited to high-risk CTV to a total dose of 60–70 Gy/30–35 fractions (median 70 Gy). The details of target definition and margins for planning target volume (PTV) has been mentioned elsewhere [7].

Of the 20 patients, 10 had NPC, six oropharyngeal cancer (OPC), and four hypopharyngeal cancer (HPC) (Table 1). Six patients were treated with neck lymph node dissection before IMRT. Most patients were treated with concurrent chemotherapy of cisplatin 80 mg/m<sup>2</sup> as a Japanese standard dose for 2 or 3 times.

All patients were immobilized with a thermoplastic mask covering the head, neck and shoulders (Type-S thermoplastic based system, MED-TEC, Orange City, IA). Computed tomography (CT) scans or positron emission tomography/CT (PET/CT) for treatment planning were obtained with contrast medium at 2 mm slice intervals from the head through the aortic arch. For all patients, treatment-planning CT or PET-CT was done twice before IMRT (CT-1) and at the third or fourth week of IMRT for the treatment planning of boost IMRT (CT-2) with a new thermoplastic mask. A new mask was made carefully to be the same bony alignment of the initial mask. Boost IMRT was started without split at the fifth week of IMRT. An integrated PET/CT simulation was performed at CT-1 for 15 patients [9].

All treatment planning data for IMRT was obtained by inverse planning with commercial treatment-planning systems (Eclipse ver.7.3.10, Varian Medical Systems International Inc., Baden, Switzerland). The IMRT beam arrangements consisted of seven co-planar beams. The prescribed dose for PTV was 70 Gy, and the following dose constraints were set on the organs at risk (OARs): maximum dose for the spinal cord, 45 Gy; maximum dose of the brain stem, 54 Gy; mean dose for at least one parotid gland, 26 Gy, although both parotid glands were tried to spare. Detailed dose constraints for IMRT planning used at our institution are described in Table 2.

#### Method of analysis

To eliminate interobserver variability, re-contouring of OARs and target volumes was performed by a single observer (TN) and validated by a single medical doctor (YN). The spinal cord was outlined without margin between the first and sixth cervical vertebra

**Table 2**  
The objective parameters used in IMRT optimization.

Target and risk organs	Dose constraints
PTV	D <sub>95</sub> = 100% (prescription dose 70 Gy) V <sub>110%</sub> < 10% of PTV D <sub>max</sub> < 120% D <sub>mean</sub> < 105%
Organs at risk	
Brain (PRV)	D <sub>max</sub> < 63 Gy
Brain stem (PRV)	D <sub>max</sub> < 54 Gy
Spinal cord (PRV)	D <sub>max</sub> < 45 Gy
Optic nerve	D <sub>max</sub> < 54 Gy
Amphiblastrode	D <sub>mean</sub> < 35 Gy
Lens	D <sub>max</sub> < 6 Gy
Inner/middle ear	D <sub>mean</sub> < 45 Gy
Oral cavity	D <sub>max</sub> < 54 Gy
Larynx	D <sub>mean</sub> < 45 Gy
Parotid gland (at least one)	D <sub>mean</sub> < 26 Gy
Non-specific region	D <sub>max</sub> < 70 Gy

Abbreviations: PTV, planning target volume; PRV, planning organ at risk volume; D<sub>max</sub>, maximum dose; D<sub>mean</sub>, mean dose; D<sub>95</sub>, dose to the 95% of the volume; V<sub>110%</sub>, Volume (%) of receiving 110% of the prescription dose.

level. Parotid glands were also outlined without margin. Utilizing PET-CT findings, the primary tumors and the largest metastatic lymph node were re-contoured without margin as gross tumor volume-p (GTV-p) and GTV-n, respectively.

IMRT plans were defined as follows: Plan-1 was the actual initial IMRT plan applied to CT-1. Plan-2 was the actual boost IMRT plan on CT-2. In addition, a Plan-3, in which the initial IMRT plan was transferred to CT2 based on carefully matched Isocenter and bony alignment, was made for this study. Dose distributions of these plans were recalculated to obtain dose-volume histograms (DVHs) of re-contoured target volumes and OARs. No optimization was performed for Plans-1, 2, and 3 after re-contouring.

The changes in volume, distance and dose were analyzed for each patient. Comparisons of these parameters on Plan-1, Plan-2 and Plan-3 were analyzed by Mann-Whitney-Wilcoxon tests.

Volumes of GTVs and bilateral parotid glands were compared between CT-1 and CT-2 with a paired samples analysis. To quantify the positional shifts of the parotid glands, we calculated the distance from the surface of the parotid glands or the retromandibular vein in the parotid glands to the midline on the slice with the largest parotid gland area.

Dosimetric parameters such as  $D_{\text{mean}}$ ,  $D_{98}$ , and  $D_2$  were evaluated for Plan-1, Plan-2, and Plan-3.  $D_{98}$  and  $D_2$  were doses to the 98% and 2% of the volume, respectively. For each IMRT plan, DVHs were calculated for GTVs and critical risk organs. Plan-3 was compared to Plan-1 to evaluate the effects of anatomic changes on dosimetric outcomes. The replanning effects for dosimetric outcomes were compared for Plan-2 and Plan-3. Dose parameters were calculated for a total prescribed dose of 70 Gy for each plan. In addition,  $D_{\text{mean}}$  (sum) of the bilateral parotid glands was calculated for each patient as follows.

$$D_{\text{mean}}(\text{sum}) = D_{\text{mean}}(\text{Plan-1}) \times (\text{initial plan dose})/70 \\ + D_{\text{mean}}(\text{Plan-2}) \times (\text{boost plan dose})/70$$

After the end of IMRT, loco-regional control and distant progression was evaluated every 3–4 months for more than 5 years by clinical examination, laryngo-pharyngeal fiberoptic, and every 6 months by head and neck MRI or CT scan, as well as thoraco-abdominal CT scan.

Late toxicities were graded according to the Common Toxicity Criteria for Adverse Events (CTCAE) version 3.0. Xerostomia was scored prospectively and recorded in the clinical chart every 3–4 months. The attending physicians (YN and TS) asked patients to follow dietary alterations and the need for a water bottle every 3–4 months, and the best grade at 12–24 months after the start of IMRT was used as an end-point.

## Results

Fig. 1(a–c) shows the volume changes in GTVs and parotid glands between CT-1 and CT-2. The mean volumes of GTV-p and GTV-n on CT-2 reached  $37.1 \pm 23.5\%$  and  $47.6 \pm 36.8\%$  compared with CT-1, respectively ( $p = 0.002$  and  $p = 0.081$ ). The volume of parotid glands also decreased to  $81.9 \pm 12.4\%$  of the initial volume with significant difference ( $p < 0.0001$ ). The lateral surface of the parotid glands shifted medially with an average of  $4.2 \pm 2.9$  mm

( $p < 0.0001$ ) on CT-2. The retromandibular vein in parotid glands shifted medially with an average of  $2.4 \pm 3.3$  mm ( $p = 0.00002$ ).

Table 3 shows dose parameters calculated for a total prescribed dose of 70 Gy for each plan.  $D_{\text{means}}$  of parotid glands in Plan-1, Plan-2 and Plan-3 were 25.4 Gy, 20.0 Gy and 30.3 Gy per 70 Gy, respectively. In addition, the average  $D_{\text{mean}}$  (sum) of the bilateral parotid glands was  $23.9 \pm 2.6$  Gy. According to the anatomical change,  $D_{\text{mean}}$  of the parotid glands increased significantly between Plan-1 and Plan-3 ( $5.0 \pm 5.1$  Gy; 119.9%,  $p < 0.0001$ ).  $D_{\text{mean}}$  of the parotid glands significantly reduced in Plan-2 compared with Plan-3 ( $10.3 \pm 3.6$  Gy; 66.0%,  $p < 0.0001$ ).

There was no statistically significant difference in the  $D_{\text{mean}}$  of the spinal cord.  $D_2$  values of the spinal cord were 37.2 Gy, 36.7 Gy and 39.1 Gy per 70 Gy, respectively. The increase in the  $D_2$  of spinal cord was statistically significant at Plan-3 compared to Plan-1 ( $1.9 \pm 2.0$  Gy; 105.4%,  $p = 0.0003$ ). The increase in  $D_2$  of the spinal cord was correlated with the volume loss of GTV-p (Spearman's correlation coefficient 0.91).  $D_2$  of the spinal cord could be reduced by Plan-2 compared with Plan-3 ( $2.4 \pm 5.2$  Gy; 93.9%,  $p = 0.0507$ ) with marginal significance. Between Plan-1 and Plan-3, there was a slight but significant increase in  $D_{\text{mean}}$  and  $D_{98}$  of GTV-p ( $0.6 \pm 0.7$  Gy;  $p = 0.0007$ ,  $0.8 \pm 0.6$  Gy;  $p < 0.0001$ ). There were no significant dose changes in  $D_{\text{mean}}$  and  $D_{98}$  of GTV-n.

Fig. 2 shows Plan-1 on CT-1 (a) and the same plan on CT-2 (Plan-3) (b) for nasopharyngeal cancer. The body size on CT-2 has shrunk, and the GTV (shown in pink) has apparently regressed. The parotid glands and spinal cord were included in the high dose region.

The median follow-up period was 57 months (range, 8–78 months). Grade of xerostomia 1–2 years after the start of IMRT could be evaluated for 15 patients. There were 12 patients with grade 0 and 3 patients with grade 1 (Table 1). No patient complained of grade 2 xerostomia in this cohort after 1–2 years.  $D_{\text{mean}}$  (sum) of parotid glands for the 12 patients with grade 0 and 3 patients with grade 1 were  $24.1 \pm 1.9$  Gy (21.6–27.8) and  $21.9 \pm 4.7$  Gy (17.5–26.8), respectively.

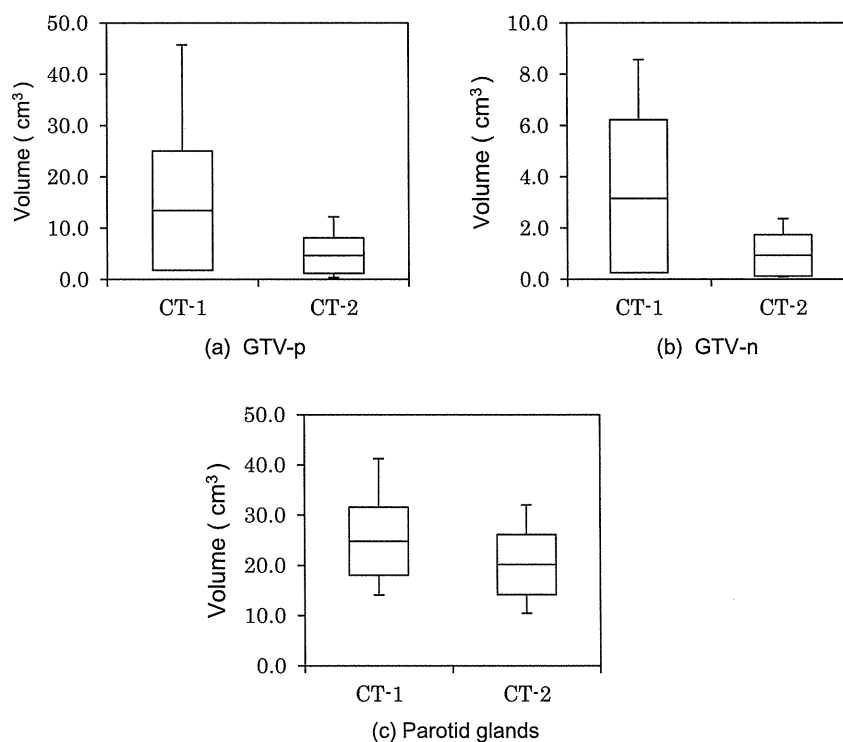


Fig. 1. (a–c). Volume changes of GTV and parotid glands between CT-1 and CT-2. The box represents standard deviation (SD), and the horizontal line in the box represents the mean of the volumes. The bar represents the range of the volumes.

**Table 3**

Dose parameters calculated for a total prescribed dose of 70 Gy for each plan.

	Index	Plan-1	Plan-2	Plan-3	Plan-3-Plan-1		Plan-3-Plan-2	
		Ave. $\pm$ SD	Ave. $\pm$ SD	Ave. $\pm$ SD	Ave. $\pm$ SD	p Value	Ave. $\pm$ SD	p Value
GTV-p	D <sub>mean</sub> (Gy)	73.2 $\pm$ 0.8	72.7 $\pm$ 0.7	73.8 $\pm$ 0.7	0.6 $\pm$ 0.7	0.0007	1.1 $\pm$ 0.8	<0.0001
	D <sub>98</sub> (Gy)	71.4 $\pm$ 0.8	71.5 $\pm$ 0.7	72.1 $\pm$ 0.9	0.8 $\pm$ 0.6	<0.0001	0.7 $\pm$ 0.6	0.0003
GTV-n	D <sub>mean</sub> (Gy)	74.3 $\pm$ 1.6	73.8 $\pm$ 0.5	74.3 $\pm$ 1.7	0.0 $\pm$ 1.5	0.9600	0.5 $\pm$ 1.2	0.3270
	D <sub>98</sub> (Gy)	72.8 $\pm$ 1.7	72.8 $\pm$ 0.8	72.6 $\pm$ 1.5	-0.2 $\pm$ 2.2	0.8150	-0.3 $\pm$ 1.5	0.6650
Parotid glands	D <sub>mean</sub> (Gy)	25.4 $\pm$ 2.2	20.0 $\pm$ 5.5	30.3 $\pm$ 5.3	5.00 $\pm$ 5.1	<0.0001	10.3 $\pm$ 3.6	<0.0001
Spinal cord	D <sub>2</sub> (Gy)	37.2 $\pm$ 5.0	36.7 $\pm$ 3.9	39.1 $\pm$ 5.2	1.9 $\pm$ 2.0	0.0003	2.4 $\pm$ 5.2	0.0507

Abbreviations: GTV-p = the volume of primary gross tumor; GTV-n = the volume of maximum metastatic lymph node; D<sub>mean</sub> = mean dose; D<sub>98</sub> = dose to the 98% of the volume; D<sub>2</sub> = dose to 2% of the volume.

Plan-1 = initial treatment plan applied on CT-1; Plan-2 = boost treatment plan on CT-2; Plan-3 = the original plan with the initial treatment plan transferred to the same anatomical position of CT-1 on CT-2.

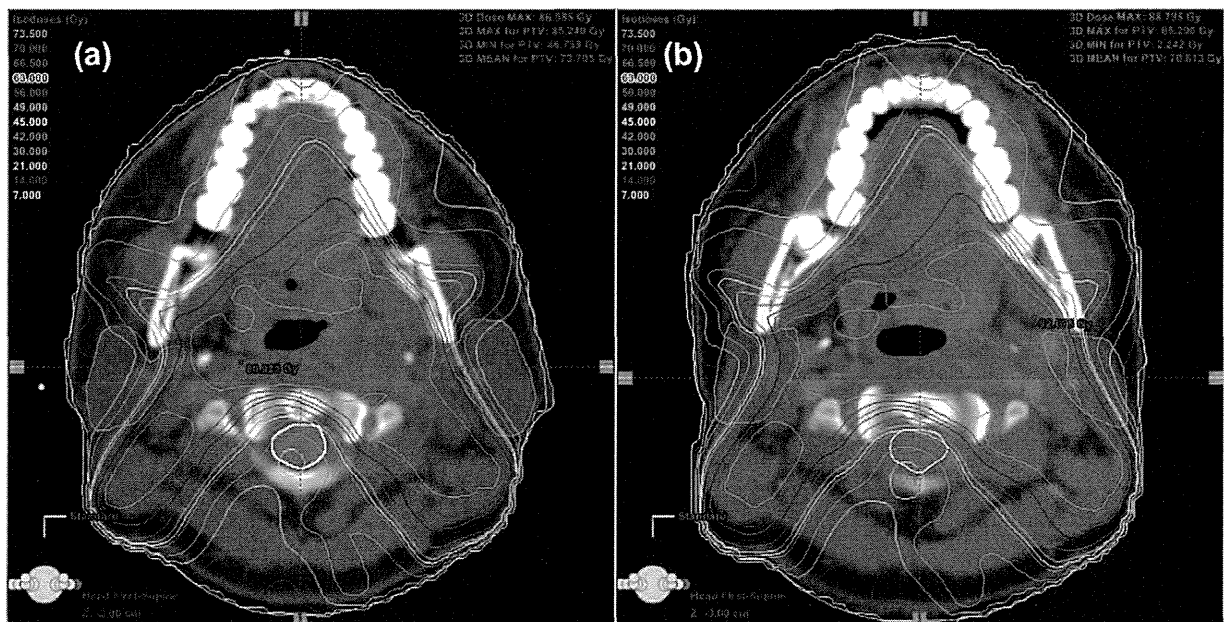


**Fig. 2.** (a) Dose distribution of the initial IMRT plan on CT-1 (Plan-1) for a patient with nasopharyngeal cancer. (b) Dose distribution of the same plan on CT-2 (Plan-3). The body size on CT-2 shrank, and the parotid glands shifted medially. A 30 Gy iso-dose line (pink) shifted to the middle of the parotid glands (orange).

Loco-regional control rates for patients with NPC and OPC/HPC were 100% and 50%, respectively. Loco-regional recurrences were noted in one patient with HPC and four patients with OPC, although no marginal recurrences were noted (Table 1).

## Discussion

Dosimetric and clinical results of our adaptive RT scheme for a two-step IMRT method for head and neck cancers were analyzed in the present study. Although there are many studies on dosimetric changes during IMRT [10–12], a few studies revealed the dosimetric changes and the clinical outcome of adaptive RT [4]. Schwartz et al. [4] performed a prospective study of adaptive RT simultaneous integrated boost (SIB) method for 22 patients with head and neck cancer, and demonstrated that one or two adaptive replanning could provide dosimetric and clinical benefit. Although one replanning was necessary for all patients, second replanning was necessary for 36% (8/22) of the patients. As the significant anatomical changes occurred during 3–4 weeks of treatment [4,5], at least one replanning (two-step) seems necessary for head and neck cancer. The advantage of a sequential two-step method compared with replanning of a SIB method [4,12] may be that the irradiated volume can be reduced in the second step boost IMRT.

Several studies have demonstrated anatomical changes during IMRT with concurrent chemotherapy for head and neck cancer [5–7,10,11]. Similar anatomical and volume changes were noted in the present study, and the position of the parotid glands shifted medially with an average of 4.2 mm. The mean volumes of the GTV-p and parotid glands on CT-2 obtained after 3–4 weeks of IMRT reached 37.1% and 81.9% respectively, compared with CT-1 with significant difference. If replanning was not performed, the parotid glands shifted toward a high dose region (Fig. 2).

In terms of dosimetric changes according to the change in body surface contour and positional changes of target and risk organs for head and neck cancer, significant changes in maximum dose of the spinal cord and D<sub>50</sub> (dose to 50% of the volume) of the parotid glands were reported by Ahn et al. [10]. They concluded a need for adaptive replanning for head and neck IMRT. In the present study, the mean dose of the parotid glands and D<sub>2</sub> of the spinal cord increased significantly on Plan-3. As a two-step IMRT method can adjust to the anatomical changes in the body surface contour and target and risk organs during IMRT treatment, this method is effective to prevent any increase in the high dose regions of the spinal cord and parotid glands. No patients complained of grade-2 or -3 xerostomia 1–2 years after IMRT. In three prospective studies on one-step IMRT using a SIB method, incidences of grade 2

or worse xerostomia at 1–2 years were reported 16.1%, 29.0%, and 39.3%, respectively [2,13,14]. Thus, our initial clinical results suggest that a two-step IMRT may be effective for preventing xerostomia.

As patients with locally advanced NPC frequently appeared with large neck lymph node swelling and as both primary tumors and neck lymph nodes regress rapidly with RT, a two-step IMRT method is especially desirable for locally advanced NPC. In fact, good loco-regional control was obtained for NPC in the present study.

In conclusion, the dosimetric advantage of a two-step IMRT method was shown for patients with head and neck cancer treated with concurrent chemotherapy. This two-step IMRT method as an adaptive RT scheme could adapt to changes in body contour, target volumes and risk organs during IMRT.

### Conflict of Interest

None.

### Acknowledgments

This study was supported in part by a Grand-in-Aid for Cancer Research (H23-009) from the Ministry of Health, Labour and Welfare of Japan, and by the National Cancer Center Research and Development Fund (23-A-21).

### References

- [1] Pow EH, Kwong DL, McMillan AS, et al. Xerostomia and quality of life after intensity-modulated radiotherapy vs. conventional radiotherapy for early-stage nasopharyngeal carcinoma: initial report on a randomized controlled clinical trial. *Int J Radiat Oncol Biol Phys* 2006;66:981–91.
- [2] Kam MK, Leung SF, Zee B, et al. Prospective randomized study of intensity-modulated radiotherapy on salivary gland function in early-stage nasopharyngeal carcinoma patients. *J Clin Oncol* 2007;25:4873–9.
- [3] Mendenhall WM, Mancuso AA. Radiotherapy for head and neck cancer; is the “next level” down? *Int J Radiat Oncol Biol Phys* 2009;73:645–6.
- [4] Schwartz DL, Garden AS, Thomas J, et al. Adaptive radiotherapy for head-and-neck cancer: initial clinical outcomes from a prospective trial. *Int J Radiat Oncol Biol Phys* 2012;83:986–93.
- [5] Barker Jr JL, Garden AS, Ang KK, et al. Quantification of volumetric and geometric changes occurring during fractionated radiotherapy for head-and-neck cancer using an integrated CT/linear accelerator system. *Int J Radiat Oncol Biol Phys* 2004;59:960–70.
- [6] Nishimura Y, Nakamatsu K, Shibata T, et al. Importance of the initial volume of parotid glands in xerostomia for patients with head and neck cancers treated with IMRT. *Jpn J Clin Oncol* 2005;35:375–9.
- [7] Nishimura Y, Shibata T, Nakamatsu K, et al. A two-step intensity-modulated radiation therapy method for nasopharyngeal cancer: the Kinki University experience. *Jpn J Clin Oncol* 2010;40:130–8.
- [8] Cannon DM, Lee NY. Recurrence in region of spared parotid gland after definitive intensity-modulated radiotherapy for head and neck cancer. *Int J Radiat Oncol Biol Phys* 2008;70:660–5.
- [9] Okubo M, Nishimura Y, Nakamatsu K, et al. Radiation treatment planning using positron emission and computed tomography (PET/CT) for lung and pharyngeal cancers: a multiple thresholds method for FDG activity. *Int J Radiat Oncol Biol Phys* 2010;77:350–6.
- [10] Ahn PH, Chen CC, Ahn AI, et al. Adaptive planning in intensity-modulated radiation therapy for head and neck cancers: single-institution experience and clinical implications. *Int J Radiat Oncol Biol Phys* 2011;80:677–85.
- [11] Zhao L, Wan Q, Zhou Y, Deng X, Xie C, Wu S. The role of replanning in fractionated intensity modulated radiotherapy for nasopharyngeal carcinoma. *Radiother Oncol* 2011;98:23–7.
- [12] Hansen EK, Bucci MK, Quivey JM, Weinberg V, Xia P. Repeat CT imaging and replanning during the course of IMRT for head-and-neck cancer. *Int J Radiat Oncol Biol Phys* 2006;64:355–62.
- [13] Toledano I, Graff P, Serre A, Boisselier P, et al. Intensity-modulated radiotherapy in head and neck cancer: results of the prospective study GORTEC 2004–03. *Radiother Oncol* 2012;103:57–62.
- [14] Nutting CM, Morden JP, Harrington KJ, et al. Parotid-sparing intensity modulated versus conventional radiotherapy in head and neck cancer (PARSPORT): a phase 3 multicentre randomised controlled trial. *Lancet Oncol* 2011;12:127–36.

# Dosimetric properties and clinical application of an a-Si EPID for dynamic IMRT quality assurance

Kenji Matsumoto · Masahiko Okumura ·  
Yoshiyuki Asai · Kouhei Shimomura ·  
Masaya Tamura · Yasumasa Nishimura

Received: 18 July 2012 / Revised: 19 November 2012 / Accepted: 20 November 2012 / Published online: 4 December 2012  
© Japanese Society of Radiological Technology and Japan Society of Medical Physics 2012

**Abstract** Dosimetric properties of an amorphous silicon electronic portal imaging device (EPID) for verification of intensity-modulated radiation therapy (IMRT) were investigated as a replacement for conventional verification tools. The portal dosimetry system of Varian's EPID (aS1000) has an integrated image mode for portal dosimetry (PD). The source-to-imager distance was 105 cm, and there were no extra buildup materials on the surface of the EPID in this study. Several dosimetric properties were examined. For clinical dosimetry, the dose distributions of dynamic IMRT beams for prostate cancer (19 patients, 97 beams) were measured by EPID and compared with the results of ionization chamber (IC) measurements. In addition, pre-treatment measurements for prostate IMRT (50 patients, 309 beams) were performed by EPID and were evaluated by the gamma method (criterion: 3 mm/3 %). The signal-to-monitor unit ratio of PD showed dose dependence, indicating ghosting effects. Tongue-and-groove effects were observed as a result of the dose difference in the measured EPID images. The results of PD for clinical IMRT beams were in good agreement with the predicted dose image with average values of 1.37 and 0.25 for  $\gamma_{\max}$  and  $\gamma_{\text{ave}}$ , respectively. The point doses of PD were slightly, but significantly, higher than the results of IC measurements ( $p < 0.05$  paired  $t$  test). However, this small difference seems clinically acceptable. This portal dosimetry

system is useful as a rapid and convenient verification tool for dynamic IMRT.

**Keywords** Portal dosimetry · EPID · IMRT quality assurance

## 1 Introduction

Advanced irradiation techniques, including intensity-modulated radiation therapy (IMRT), require extensive dose verification measurements. The delivery of IMRT beams employs several different techniques, including physical compensators, the step-and-shoot technique [1], and a dynamic multi-leaf collimator (MLC) [2–5]. Verification of dose distributions when these IMRT techniques are used requires at least two-dimensional (2D) dosimetry tools, and has been performed with use of radiographic film [6, 7]. This verification procedure includes recalculation of IMRT plans, set-up of radiographic films on linear accelerators, film processing and digitization, and comparisons of the calculated and measured dose distribution, which is a time-consuming procedure.

Amorphous silicon electronic portal imaging devices (a-Si EPID) were originally designed for patient set-up verification. Because portal images contain dosimetric information, The a-Si EPID has also been used for dose verification recently. 2D verification images can be acquired rapidly without re-entering of the treatment room. 2D detector dosimetry devices have also been proposed based on an ionization chamber or diode array for pre-treatment verification of IMRT [8–11]. Whereas good agreement has been reported at specific points or along profiles, these two approaches have limited resolution (0.7–1.4 cm grid spacing) and require additional set-up

---

K. Matsumoto (✉) · M. Okumura · Y. Asai · K. Shimomura  
Faculty of Medicine, Central Radiological Service,  
Kinki University, 377-2 Ohno-higashi, Osaka-Sayama,  
Osaka 589-8511, Japan  
e-mail: kenji356@me.com

M. Tamura · Y. Nishimura  
Faculty of Medicine, Department of Radiation Oncology,  
Kinki University, Osaka-Sayama, Japan

time. The EPID has the advantage of higher resolution, and it is already fixed to linear accelerators without needing any additional hardware. Because many radiotherapy departments have invested in portal imagers for patient set-up verification in recent years, it would be useful if the same device could be used also for accurate dose verification.

Early generations of EPIDs consisted of a liquid ion chamber and camera-based fluoroscopic units. The EPID images had poorer contrast and poorer spatial resolution than radiographic films [12–14]. The latest generation of EPIDs has an array of photodiode detectors on an amorphous silicon glass substrate (a-Si EPID). The a-Si EPID produces images that have improved spatial resolution and better contrast than the early generation EPIDs, because the device has a higher detective quantum efficiency.

The dosimetric properties of the a-Si EPID and its applicability to dynamic IMRT verification have been reported [15–21]. One of the approaches to EPID dosimetry was to convert an a-Si EPID image to a dose to water [22]. In this approach, Monte Carlo methods were applied for calculation of the predicted dose distribution at the plane of the EPID. Another approach was the back-projection method, which needs in-house programs for a-Si EPID dosimetry [23]. Each study explored the possibility of EPID dosimetry by use of a special in-house calculation algorithm.

Varian's portal dosimetry (PD) system has image acquisition hardware/software (IDU-20/IAS3) and does not need in-house software for calculation of the predicted dose image (PDI). This commercially available portal dosimetry system was commissioned for the quality assurance (QA) of IMRT treatment plans. Properties investigated were the linearity of the frame number, the linearity of the EPID signal-to-MU ratio, the influence of beam hold-off, the influence of MLC shapes, and the dose accuracy. As for clinical dosimetry, pretreatment verification for the prostate IMRT plan was performed by PD. Our aim in this study was to evaluate the dosimetric properties and application of the PD system as an IMRT verification tool.

## 2 Methods

An a-Si EPID (aS1000, Varian Medical Systems, Palo Alto, CA) consists of a 1 mm copper metal plate, a 134 mg/cm<sup>2</sup> gadolinium oxysulfide phosphor screen (Kodak, Lanex fast B) that includes a 0.18 mm polyester reflector and a 40 × 30 cm<sup>2</sup> (1,024 × 768 pixels) a-Si array. The 1 mm copper plate is equal to an 8-mm thickness of water and serves as buildup for the incoming radiation. The pixel pitch of aS1000 is 0.39 × 0.39 mm<sup>2</sup> at a source-to-image distance (SID) of 100 cm, which shows higher resolution than that of aS500. The aS1000 was

equipped with a Varian 21EX linear accelerator (hereafter abbreviated as 21EX, Varian Medical Systems). 21EX has a Millennium 120 (60 pair) MLC system. Investigations of dosimetric properties and pre-treatment verification of the clinical IMRT plan were performed at an SID of 105 cm without extra buildup materials, with use of a 10 MV photon beam energy and a gantry angle of 0°. The SID of 105 cm is the measurement distance recommended by the manufacturer. The portal dose prediction (PDP) algorithm was implemented in the treatment planning system (TPS). We used the TPS (Varian Eclipse versions 7.3.10 and 10.0.24) to calculate the PDI. Recently, Eclipse was upgraded to version 10.0.24 from version 7.3.10. In the PD system, measured EPID dose images were compared with the PDI calculated from the fluence map of the clinical IMRT plan for verification of the IMRT plan.

### 2.1 Frame acquisition accuracy

For measurement of EPID dose images, Varian's EPID system uses an integrated image mode. In this study, EPID images were acquired by use of this mode. An EPID image was acquired as a frame during irradiation. Accumulated frames were displayed as a single dose image after irradiation was completed. The preset rate of frame acquisition was 9.574 frames per second (fps) for 200–600 MU/min and 5.460 fps for 100 MU/min. The image acquisitions were controlled by the central processing unit (CPU) of image acquisition system version 3 (IAS3) located in the treatment room. To verify the accuracy of the frame acquisition by IAS3, we measured the frame number with MU set values of 1–999, and dose rate settings of 200 and 500 MU/min with a 10 × 10 cm<sup>2</sup> open field. For each MU setting, frame was continuously acquired during the irradiation, and they were quantified for each dose rate for analysis.

### 2.2 Accuracy of the EPID signal-to-MU ratio

The PD system requires several calibrations processes to be used as a dosimetric tool. The calibration procedure was performed according to a calibration protocol recommended by Varian Medical Systems. This calibration procedure has three steps, namely, acquisition of dark-field (DF) images, acquisition of flood-field (FF) images, and dose calibration. First, the DF image was acquired with no radiation and the pixel offsets were recorded. The FF image was recorded with an open-field irradiation (40 × 30 cm<sup>2</sup>) for determination of the difference in sensitivity for each pixel. After the acquisition of DF and FF images, an absolute dose calibration was performed. The EPID signal was calibrated with irradiation delivery of 100 MU and a 10 × 10 cm<sup>2</sup> jaw setting. Each calibration

was performed with the dose rate of the verified IMRT plan. Because the PDI was calculated at an SID of 100 cm, a correction factor of 0.907 (i.e., inverse square of SID 105 cm) was applied to the measured EPID signal. The corrected EPID signal was converted to a calibration unit (CU). The CU is a unique absolute-dose unit of the PD (1 CU = 100 MU). The calibration procedure was performed routinely for every measurement.

To investigate the linearity of the signal-to-MU ratio in a range of 1–999 MU, we acquired EPID images using an open square field ( $10 \times 10 \text{ cm}^2$ ). Two dose rates, 200 and 500 MU/min, were employed. CU values of EPID images were obtained as an average value of a  $1 \times 1 \text{ cm}^2$  region at the center of the irradiation field. As for the control, ionization chamber (IC) measurements were also performed with the same beam-delivery settings. The cylindrical IC used was a farmer type N30001 model (PTW, Hicksville, NY) of  $0.6 \text{ cm}^3$  volume. The IC measurements were recorded in a water tank with the IC positioned at a 2.5-cm water depth and a source-detector distance (SDD) of 102.5 cm. To improve the signal-to-noise ratio, we performed IC measurements at a 2.5-cm water depth ( $d_{\text{max}}$  of 10 MV). These results were calculated as the signal-to-MU ratio and compared.

The essential factors for EPID-based dosimetry are accuracy of the imager calibration and that of the calculation algorithm of the PDI. To investigate the accuracy of the PDP algorithm, we also calculated the corresponding PDI. Because the PDI can be calculated only for dynamic IMRT fields, a  $10 \times 10 \text{ cm}^2$  jaw setting and a dynamic MLC moving outside the open field were employed. The CU values of the PDI were also measured as an average value of a  $1 \times 1 \text{ cm}^2$  area on the central axis. The measured and calculated CU values were compared.

### 2.3 Response to dose-rate fluctuations

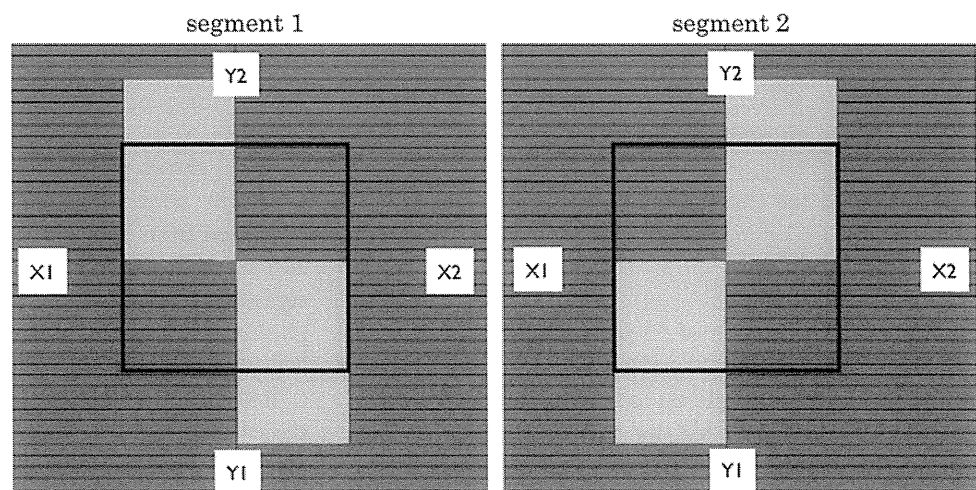
The EPID was calibrated with a fixed dose rate similar to that of the original IMRT plan. When the MLC cannot reach a pre-defined position with maximum leaf speed, the accelerator reduces the dose rate until the MLC reaches a pre-defined position. This phenomenon causes large dose-rate fluctuations during IMRT beam delivery. This phenomenon may affect the measured EPID signals, because this portal dosimetry system is designed and calibrated under a stable dose-rate condition.

Effects of beam hold-offs were examined with use of a stepwise IMRT test pattern. We used two dose-rate settings of 100 and 600 MU/min to deliver the test field with 100 MU. The maximum leaf speed was 2.5 cm/s. Measurements at each dose-rate setting were performed under the same condition as that for the pre-treatment verification measurement. Two profiles along the leaf movement direction in the measured EPID images were obtained and compared.

### 2.4 Effect of MLC shapes

The MLC has several characteristics such as rounded-leaf-end and tongue-and-groove (T&G) shapes. Several studies investigated the specifications of MLC transmission [24, 25]. At our institution, the rounded-leaf-end transmission value was measured according to the method reported by Arnfield et al. and it was incorporated into the TPS as a calculation parameter. The T&G shape can reduce the transmission passing from each leaf side when the leaves are positioned side by side. However, if a single leaf side contributes to form a radiation field during IMRT irradiation, an unnecessary dose reduction may occur. To evaluate the effects of MLC characteristics on portal dosimetry, we examined a test field using a step-and-shoot

**Fig. 1** MLC settings for test fields with  $10 \times 10 \text{ cm}^2$  jaw sizes. Two segments of MLC were delivered with use of a step-and-shoot IMRT technique



IMRT technique. Two MLC segments were planned sequentially in step-and-shoot mode. The leaf settings of the two segments are shown in Fig. 1. The test field was measured with 100 MU and divided into 50 MU for each segment similar to the pre-treatment verification condition. The PDIs were also calculated by the PDP algorithm of both versions 7.3.10 and 10.0.24. Two dose profiles parallel and perpendicular to the movement direction of the MLC were measured and compared with the PDI.

### 2.5 Dose accuracy of portal dosimetry

To apply the PD system as a reliable dosimetric tool, it is necessary to confirm whether it has an accuracy equivalent to that of the traditional verification tool. Pre-treatment verification of 19 clinical IMRT plans (97 beams) was performed by EPID and IC. The clinical IMRT plans for the prostate were calculated with use of a dynamic MLC technique, with 5–7 beams of 10 MV X-rays. These were planned by use of a pencil-beam convolution algorithm and a 300 MU/min dose rate so that beam hold-off was avoided. A Farmer type N30001 model (PTW, Hicksville, NY) of 0.6-cm<sup>3</sup> volume was used. To calculate the IC dose, we obtained CT images of a homogeneous IMRT phantom with IC. Each IMRT beam was transposed into the CT image within the TPS. The IC was positioned at high-dose areas in the IMRT dose distribution for improvement of the signal-to-noise ratio. Each IMRT field was recalculated with a gantry angle of 0° and with the same number of MUs as in the original IMRT plan. IC measurements were performed at the same calculation position. The ratio between the IC-measured dose ( $IC_{meas}$ ) and the TPS-calculated dose ( $Plan_{calc}$ ) was calculated. After EPID calibrations, PD measurements were performed. A point dose on the EPID image was selected at the same position as that of the IC. For every IMRT plan, the verification plan was recalculated by use of PDP algorithm version 7.3.10. The measured EPID doses were compared with the PDI doses. The ratio between the EPID-measured dose ( $EPID_{meas}$ ) and the PDI-calculated dose ( $PDI_{calc}$ ) was calculated for each beam. Finally, ratios of dose differences for  $\Delta EPID$  ( $\Delta EPID = EPID_{meas}/PDI_{calc}$ ) and  $\Delta IC$  ( $\Delta IC = IC_{meas}/plan_{calc}$ ) were compared and analyzed.

### 2.6 Clinical application

Pre-treatment verification of 50 prostate IMRT plans with 309 beams was performed by PD. EPID dose images were measured at a gantry angle set to 0° with the original MU. The PDIs were calculated by PDP algorithm version 7.3.10. The measured and calculated dose images were compared by use of the gamma analysis function provided in the Eclipse software [26]. Comparison criteria were set

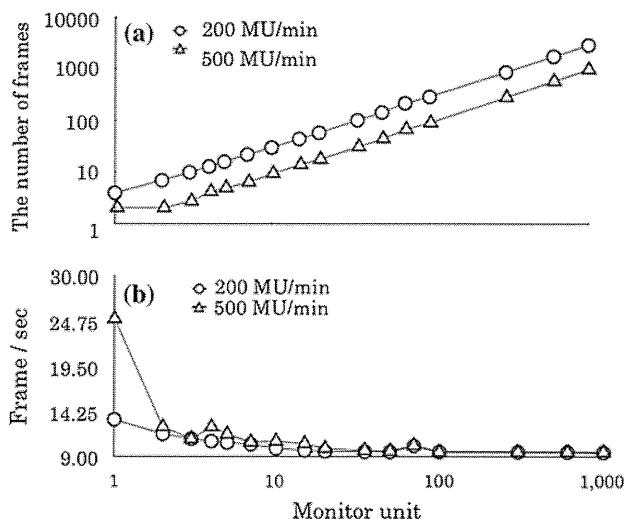


**Fig. 2** a Linearity of acquired frame number with the monitor unit. Dose rates selected were 200 and 500 MU/min. b Frame acquisition rate calculated from the frame number. Preset value of the frame acquisition rate was set as 9.574 fps for each dose rate

to  $\pm 3\%$  for dose difference and  $\pm 3$  mm for distance to agreement. The 10% threshold of the maximum dose was utilized. Maximum gamma ( $\gamma_{max}$ ) and average gamma ( $\gamma_{avg}$ ) values of 309 IMRT beams were analyzed.

## 3 Results

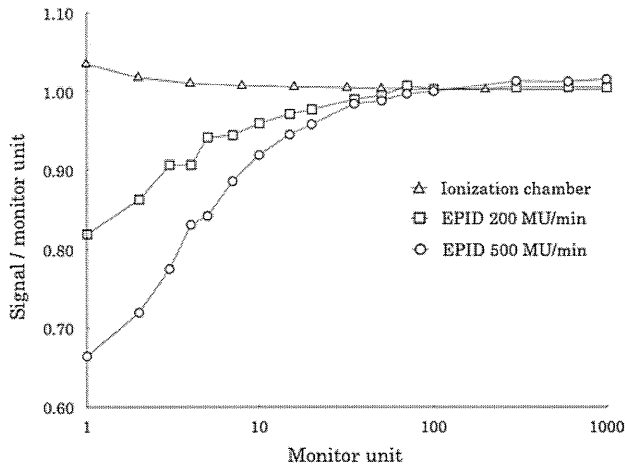
### 3.1 Frame acquisition accuracy

The relationship between the number of frames and the MUs delivered is shown in Fig. 2a. Below 3 MU of 500 MU/min, the acquisition frame number per MU was not linear. The frame/s increased up to 25.0. However, this increase in fps was observed only below 3 MU and in high-dose-rate (500 MU/min) beam-delivery situations. The acquisition frame number per MU was stable at 3 MU or more for both dose rates (Fig. 2b).

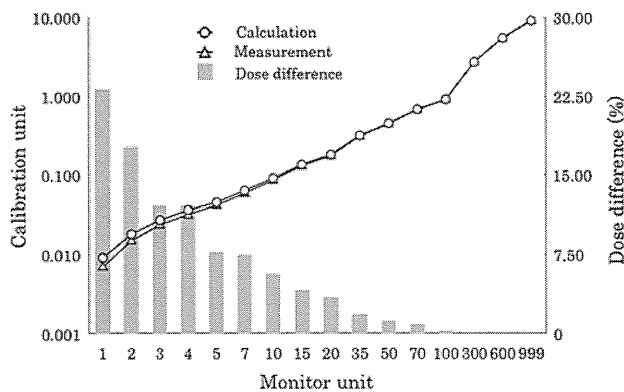
### 3.2 Accuracy of the signal-to-MU ratio on EPID

Figure 3 shows signal/MU ratios for EPID and IC. Each ratio was normalized at 100 MU. The signal/MU ratio decreased from 1.0 at MUs of <70. At a high dose rate of 500 MU/min, this tendency was more apparent. In contrast, signal/MU ratios were stable at all MUs for IC. The ghosting effect was observed in the EPID results, and the dependence on the dose rate was identified.

Results for the PDP algorithm calculation accuracy are shown in Fig. 4. The percentage dose differences between measured and calculated CU values were within  $\pm 0.5\%$  at 100 MU or more. Measured CU values of <70 MU were systematically below the calculated CU value. Eventually, in



**Fig. 3** Signal-to-monitor unit ratios measured by EPID and an ionization chamber. The ionization chamber reading was recorded for determination of the delivery system stability. Each curve was normalized to 1.0 at 100 MU



**Fig. 4** Calculation accuracy of the PDP algorithm compared with measurements. Dose differences between calculation and measurement are shown as a bar graph

PD, combination of ghosting effect and PDP algorithm calculation accuracy was effective on the situation of small MU delivery.

### 3.3 Response to dose-rate fluctuations

Measured profiles of a test pattern are shown in Fig. 5. The leaf speeds and dose rate were stable during irradiation at 100 MU/min. At a dose rate of 600 MU/min, the dose rate fluctuated between 130 and 600 MU/min when the leaf speed reached 2.5 cm/s. This phenomenon may also occur in clinical IMRT plans. There was no difference in measured CUs at the two different dose rates.

### 3.4 Effect of MLC shapes

Measured EPID images for the two MLC segments delivered sequentially in step and shoot modes are shown in

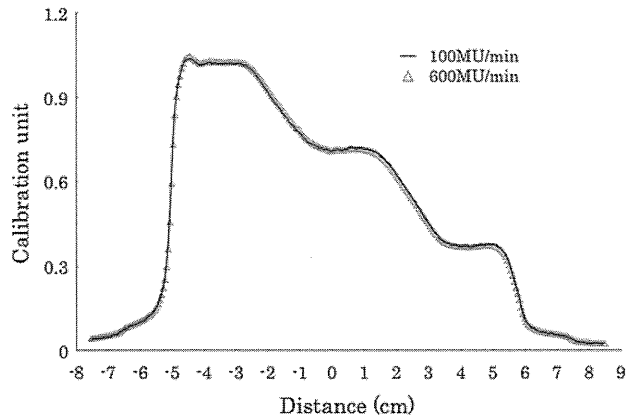


**Fig. 5** Effect of dose-rate fluctuations during intensity modulated beam delivery. The stepwise test pattern was delivered by 100 MU at 100 and 600 MU/min. There was beam hold-off during beam delivery of 600 MU/min

Fig. 6a. The leaf settings of the two segments are shown in Fig. 1. Profiles perpendicular (inline) and parallel (cross-line) to the leaf movement direction are shown in Fig. 6b and c, respectively. Each profile was compared with the calculation by the PDP algorithm. Versions of the PDP calculation algorithm used were 7.3.10 and 10.0.24. On the crossline profile, the dose discrepancy between measured and calculated values for versions 7.3.10 and 10.0.24 was 2.0 and 0.4 %, respectively. The location of this discrepancy just corresponded to the leaf end. This result indicates that the rounded leaf end value employed at our clinic seems correct and was calculated accurately. For the inline profile, calculation of PDP version 7.3.10 did not reflect the T&G effects, and the calculated dose exceeded 21 % of the measured dose ( $1.4 \gamma_{\max}$  value). However, with the latest PDP version, 10.0.24, the T&G effect could be calculated.

### 3.5 Dose accuracy of portal dosimetry

Point dose differences between PD and IC measurements for 19 prostate IMRT plans with 97 beams are shown in Fig. 7. A positive number indicates that the measured dose was higher than the calculated values. The averaged values of  $\Delta IC$  and  $\Delta EPID$  were  $0.5 \pm 0.9$  % (average  $\pm$  SD) and  $1.4 \pm 1.0$  %, respectively.  $\Delta EPID$  was systematically and significantly higher than  $\Delta IC$  ( $p < 0.05$ , paired  $t$  test).

### 3.6 Clinical application

Histograms of average and maximum  $\gamma$  values for all 309 IMRT beams are shown in Fig. 8. Good agreement between the predicted and measured dose images was observed when we used the 3 mm and 3 %  $\gamma$  criteria. The 10-% threshold was enough to take into account the ghosting effect, because that effect acted on the low-dose

**Fig. 6** MLC commissioning test of the PDP calculation algorithm. Two versions were used, 7.3.10 and 10.0.24.  
**a** Measured dose image of the test IM beam by use of Fig. 1 MLC pattern. **b** Result of inline profile comparing calculated and measured values. **c** Result of crossline profile comparing calculated and measured values

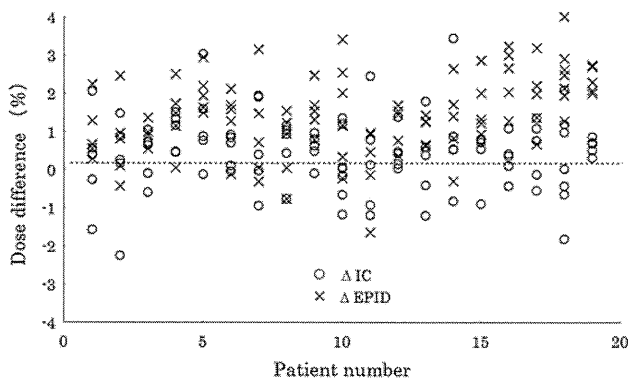
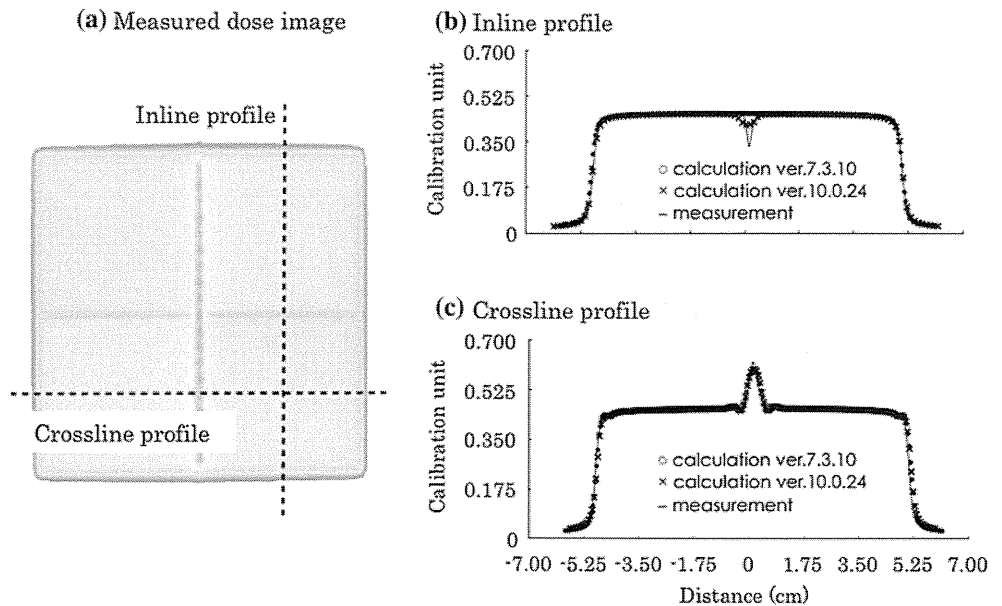


**Fig. 7** Point dose difference between PD and IC measurements for 19 prostate IMRT plans (97 beams). Each result was compared with calculated values. A *positive number* indicates that the measured dose was higher than the calculated value

area. The maximum  $\gamma_{max}$  and  $\gamma_{avg}$  of the 309 beams were 3.1 and 0.41, respectively. The average  $\gamma_{max}$  and  $\gamma_{avg}$  of the 309 beams were  $1.37 \pm 0.42$  and  $0.26 \pm 0.11$ , respectively. There were 10 fields (3.2 %) with errors of  $\gamma_{max} > 2.0$ . In these fields, the measured doses were 6–18 % lower than the calculated dose at small points.

**4 Discussion**

The present study demonstrated that a PD system could be used for verification of IMRT dose delivery. First, the dosimetric properties of a-Si EPID were investigated. The acquisition frame rate was measured, and the acquisition frame number per MU was stable at 3 MU or more for both dose rates (Fig. 2b). The previous image acquisition CPU (IAS2) had a delay between each acquired image due to

transfer of the image from the acquisition CPU to the disk and database [15]. This delay (i.e., dead time) was not fixed and could be more than 2.0 s. This delay resulted in image lag (i.e., loss of EPID signal) and inaccurate verification results. The IAS3 performance was different from that of the previous version, and there was no image lag during acquisition. Nonlinearity of the EPID response to MUs was observed in the low-MU region of this portal dosimetry system (Fig. 3). This was consistent with previous reports suggesting that the nonlinearity (known as ghosting effect) depends on the exposure and/or acquisition time [27–29]. The acquisition time dependence or ghosting effects are fundamental properties of the a-Si based EPID.

The calculation accuracy of the PDP algorithm was also investigated. The calculated CU was underestimated in a range of <70 MU. However, in a range of more than 70 MU, the differences between measured and calculated values were within 0.5 %. This result could be due to the fact that the EPID dose calibration was performed at 100 MU. Inaccuracy of the PD in a range of <70 MU may be attributed to a poor EPID response due to ghosting effects in the small-MU region.

Dose-rate fluctuations can occur during IMRT delivery; therefore, it is important to confirm the effect of dose rate fluctuations in PD. Intensity-modulated stepwise test patterns were delivered at 100 and 600 MU/min. Although the dose rate was stable during irradiation at 100 MU/min, it fluctuated between 130 and 600 MU/min when the leaf speed reached 2.5 cm/s. There was no difference in measured CUs at the two dose rates of 100 and 600 MU/min (Fig. 5), which means that dose-rate fluctuation did not affect the PD system.

Modeling of the MLC was commissioned with use of the IMRT test pattern shown in Fig. 1. T&G effects caused

**Fig. 8** Histogram of average and maximum  $\gamma$  values with use of 3 mm and 3 % tolerance, for 309 IMRT prostate fields. Measured and calculated dose distributions agreed well overall, with average  $\gamma = 0.26$ , and maximum  $\gamma = 3.0$

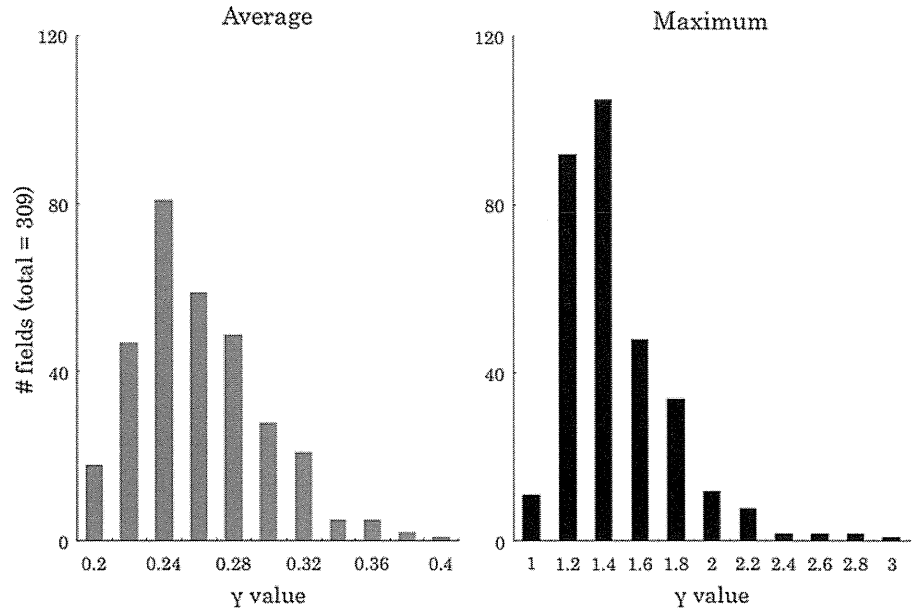
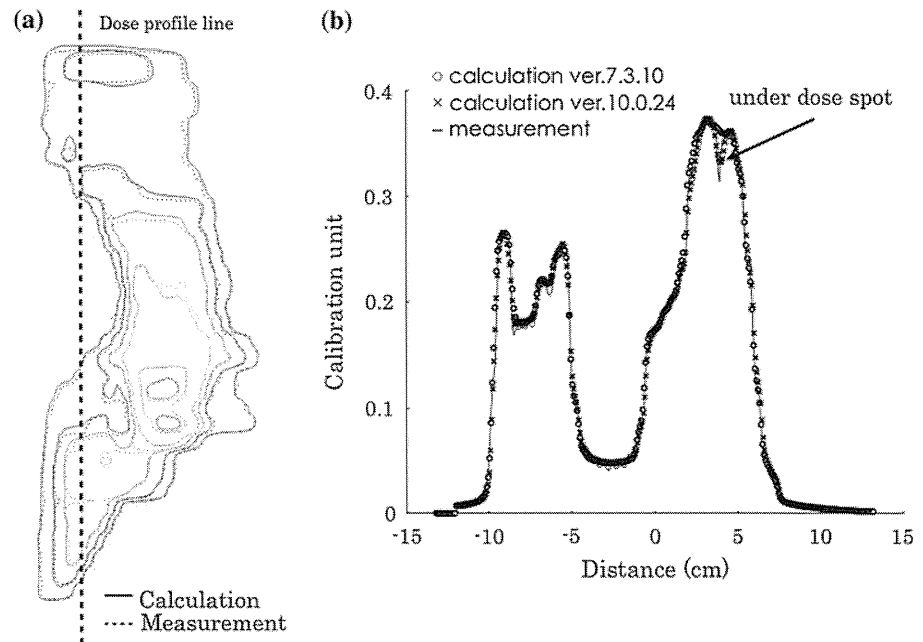


**Fig. 9** Results of prostate IMRT verification by use of PDP calculation algorithm versions 7.3.10 and 10.0.24. **a** Measured and calculated dose distribution. *Solid lines* and *dashed lines* are calculation (PDP calculation algorithm version 7.3.10) and measurement, respectively. **b** Comparison of three dose profiles along with the *bold dashed line* in **a**



a large under dosage, and the maximum dose difference was above 20 % in this particular case (Fig. 6). Similar results were observed in our past film measurements. PDP algorithm version 7.3.10 could not calculate the PDI including T&G effects; thus, the gamma value increased when intensity-modulated beams had a single leaf movement. A large discrepancy from T&G effects was occasionally observed in the results of clinical IMRT verification, and an example is shown in Fig. 9. This IMRT treatment plan was used for prostate cancer with metastases of lymph nodes in the pelvis. This plan, therefore, had a large field and more complex leaf movement than ordinary

prostate IMRT treatment plans. An under-dose spot was detected in PD, although no under-dose spot was observed in the dose distribution calculated by PDP algorithm version 7.3.10 (Fig. 9b). However, with the PDP calculation algorithm version 10.0.24, T&G effects in PDI can be calculated. T&G effects appear as a line shape moving in the direction of the MLC. Because under-dose spots due to T&G effects can be present in clinical treatment beam delivery, detection of T&G effects is important for quality control of IMRT.

The clinical applicability of PD was investigated with use of clinical IMRT beams for prostate cancer. The point

dose ratios of  $\Delta IC$  and  $\Delta EPID$  were  $0.5 \pm 0.9 \%$  (average  $\pm$  SD) and  $1.4 \pm 1.0 \%$ , respectively, with the difference being significant. Although  $EPID_{meas}$  was slightly higher than  $PDI_{calc}$ , the difference was acceptable clinically. This result suggested that PD is applicable for IMRT verification with the same accuracy as that of IC measurement. As a clinical application of PD, 309 prostate IMRT beams were verified. PDI calculated by PDP algorithm version 7.3.10 was used. The average values of  $\gamma_{max}$  and  $\gamma_{avg}$  were  $1.37 \pm 0.42$  and  $0.26 \pm 0.11$ , respectively. Similar values of  $\gamma_{max}$  and  $\gamma_{avg}$  were reported for one PD study [30], and these values seem clinically acceptable. Although 10 fields of  $\gamma_{max} > 2.0$  were noted in the present study,  $\gamma_{max}$  exceeded 2.0 only in a small portion of the fields. Recalculation with PDP calculation version 10.0.24 was performed for the 10 fields, and the maximum gamma value of all 10 fields became  $\gamma_{max} < 2.0$ . As the T&G effect was considered in the PDP calculation with version 10.0.24, a more accurate dose distribution was obtained compared with that for PDP algorithm version 7.3.10. Thus, the average gamma values in the present study were within a clinically acceptable range. Our PD system for each IMRT field dose distribution is useful in clarifying the reasons for any error.

In terms of the working time for verification of IMRT, it usually took 5 or 6 h to perform pretreatment IMRT verification with conventional film and IC measurements in our department. After we adopted the PD system, analysis of one clinical IMRT plan could be performed within 30 min. The waiting time between CT scanning for the treatment plan and the start of IMRT was also shortened, from 7 to 4 days.

## 5 Conclusion

Portal dosimetry including calibration, measurement, and analysis of one clinical IMRT plan could be performed within 30 min; this has a significant positive impact in a busy clinical environment. The PD system is a useful and fast method of dosimetry for both medical staff and patients.

**Acknowledgments** This study was supported in part by a Grant-in-Aid for Clinical Cancer Research (H23-009) from the Ministry of Health, Labour and Welfare of Japan, and by the National Cancer Center Research and Development Fund (23-A-21).

## References

- Xia P, Verhey LJ. Multileaf collimator leaf sequencing algorithm for intensity modulated beams with multiple static segments. *Med Phys.* 1998;25(8):1424–34.
- Convery DJ, Webb S. Generation of discrete beam-intensity modulation by dynamic multileaf collimation under minimum leaf separation constraints. *Phys Med Biol.* 1998;43(9):2521–38.
- Spirou SV, Chui CS. Generation of arbitrary intensity profiles by dynamic jaws or multileaf collimators. *Med Phys.* 1994;21(7):1031–41.
- Stein J, Bortfeld T, Dorschel B, Schlegel W. Dynamic X-ray compensation for conformal radiotherapy by means of multi-leaf collimation. *Radiother Oncol.* 2004;32(2):163–73.
- Wang X, Spirou S, LoSasso T, Stein J, Chui CS, Mohan B. Dosimetric verification of intensity-modulated fields. *Med Phys.* 1996;23(3):317–27.
- Bucciolini M, Buonamici FB, Casati M. Verification of IMRT fields by film dosimetry. *Med Phys.* 2004;31(1):161–8.
- Ju SG, Ahn YC, Huh SJ, Yeo IJ. Film dosimetry for intensity modulated radiation therapy: dosimetric evaluation. *Med Phys.* 2002;29(3):351–5.
- Jursinic PA, Nelms BE. A 2-D diode array and analysis software for verification of intensity modulated radiation therapy delivery. *Med Phys.* 2003;30(5):870.
- Poppe B, Blechschmidt A, Djouguela A, Kollhoff R, Rubach A, Willborn KC, et al. Two-dimensional ionization chamber arrays for IMRT plan verification. *Med Phys.* 2006;33(4):1005–15.
- Looe HK, Harder D, Ruhmann A, Willborn KC, Poppe B. Enhanced accuracy of the permanent surveillance of IMRT deliveries by iterative deconvolution of DAVID chamber signal profiles. *Phys Med Biol.* 2010;55(14):3981–92.
- Poppe B, Looe HK, Chofor N, Ruhmann A, Harder D, Willborn KC. Clinical performance of a transmission detector array for the permanent supervision of IMRT deliveries. *Radiother Oncol.* 2010;95(2):158–65.
- Yin FF, Schell MC, Rubin P. Input/output characteristics of a matrix ion-chamber electronic portal imaging device. *Med Phys.* 1994;21(9):1447–54.
- Zhu Y, Jiang XQ, Van Dyk J. Portal dosimetry using a liquid ion chamber matrix: dose response studies. *Med Phys.* 1995;22(7):1101–6.
- Essers M, Hoogervorst BR, van Herk M, Lanson H, Mijnheer BJ. Dosimetric characteristics of a liquid-filled electronic portal imaging device. *Int J Radiat Oncol Biol Phys.* 1995;33(5):1265–72.
- Greer PB, Popescu CC. Dosimetric properties of an amorphous silicon electronic portal imaging device for verification of dynamic intensity modulated radiation therapy. *Med Phys.* 2003;30(7):1618–27.
- Greer PB. Correction of pixel sensitivity variation and off-axis response for amorphous silicon EPID dosimetry. *Med Phys.* 2005;32(12):3558–68.
- Greer PB, Vial P, Oliver L, Baldock C. Experimental investigation of the response of an amorphous silicon EPID to intensity modulated radiotherapy beams. *Med Phys.* 2007;34(11):4389–98.
- Greer PB, Barnes MP. Investigation of an amorphous silicon EPID for measurement and quality assurance of enhanced dynamic wedge. *Phys Med Biol.* 2007;52(4):1075–87.
- McCurdy BMC, Greer PB. Dosimetric properties of an amorphous-silicon EPID used in continuous acquisition mode for application to dynamic and arc IMRT. *Med Phys.* 2009;36(7):3028–38.
- Gustafsson H, Vial P, Kuncic Z, Baldock C, Denham JW, Greer PB. Direct dose to water dosimetry for pretreatment IMRT verification using a modified EPID. *Med Phys.* 2011;38(11):6257–64.
- Sharma DS, Mhatre V, Heigrum M, Talapatra K, Mallik S. Portal dosimetry for pretreatment verification of IMRT plan: a comparison with 2D ion chamber array. *J Appl Clin Med Phys.* 2010;11(4):238–48.

22. Warkentin B, Steciw S, Rathee S, Fallone BG. Dosimetric IMRT verification with a flat-panel EPID. *Med Phys.* 2003;30(12):3143–55.
23. Wendling M, Louwe RJW, McDermott LN, Sonke J–J, van Herk M, Mijnheer BJ. Accurate two-dimensional IMRT verification using a back-projection EPID dosimetry method. *Med Phys.* 2006;33(2):259–73.
24. LoSasso T, Chui CS, Ling CC. Physical and dosimetric aspects of a multileaf collimation system used in the dynamic mode for implementing intensity modulated radiotherapy. *Med Phys.* 1998;25(10):1919–27.
25. Arnfield MR, Siebers JV, Kim JO, Wu Q, Keall PJ, Mohan R. A method for determining multileaf collimator transmission and scatter for dynamic intensity modulated radiotherapy. *Med Phys.* 2000;27(10):2231–41.
26. Low DA, Harms WB, Mutic S, Purdy JA. A technique for the quantitative evaluation of dose distributions. *Med Phys.* 1998;25(5):656–61.
27. McDermott LN, Louwe RJW, Sonke JJ, van Herk MB, Mijnheer BJ. Dose–response and ghosting effects of an amorphous silicon electronic portal imaging device. *Med Phys.* 2004;31(2):285–95.
28. Winkler P, Hefner A, Georg D. Dose-response characteristics of an amorphous silicon EPID. *Med Phys.* 2005;32(10):3095–105.
29. McDermott LN, Nijsten SMJJG, Sonke JJ, Partridge M, van Herk M, Mijnheer BJ. Comparison of ghosting effects for three commercial a-Si EPIDs. *Med Phys.* 2006;33(7):2448–51.
30. Roxby KJ, Crosbie JC. Pre-treatment verification of intensity modulated radiation therapy plans using a commercial electronic portal dosimetry system. *Australas Phys Eng Sci Med.* 2010;33(1):51–7.

# A prospective clinical trial of tumor hypoxia imaging with $^{18}\text{F}$ -fluoromisonidazole positron emission tomography and computed tomography (F-MISO PET/CT) before and during radiation therapy

Izumi TACHIBANA<sup>1,\*</sup>, Yasumasa NISHIMURA<sup>1</sup>, Toru SHIBATA<sup>1</sup>, Shuichi KANAMORI<sup>1</sup>, Kiyoshi NAKAMATSU<sup>1</sup>, Ryuta KOIKE<sup>1</sup>, Tatsuyuki NISHIKAWA<sup>1</sup>, Kazuki ISHIKAWA<sup>1</sup>, Masaya TAMURA<sup>1</sup> and Makoto HOSONO<sup>2</sup>

<sup>1</sup>Department of Radiation Oncology, Kinki University Faculty of Medicine, Osaka-Sayama, Japan

<sup>2</sup>Institute of Advanced Clinical Medicine, Kinki University Faculty of Medicine, Osaka-Sayama, Japan

\*Corresponding author. Department of Radiation Oncology, Kinki University Faculty of Medicine, 377-2, Ohno-Higashi, Osaka-Sayama, Osaka 589-8511, Japan. Tel: +81-72-366-0221 (ext. 3132); Fax: +81-72-368-2388; Email: izu917@med.kindai.ac.jp

(Received 31 August 2012; revised 21 March 2013; accepted 22 March 2013)

To visualize intratumoral hypoxic areas and their reoxygenation before and during fractionated radiation therapy (RT),  $^{18}\text{F}$ -fluoromisonidazole positron emission tomography and computed tomography (F-MISO PET/CT) were performed. A total of 10 patients, consisting of four with head and neck cancers, four with gastrointestinal cancers, one with lung cancer, and one with uterine cancer, were included. F-MISO PET/CT was performed twice, before RT and during fractionated RT of approximately 20 Gy/10 fractions, for eight of the 10 patients. F-MISO maximum standardized uptake values (SUV<sub>max</sub>) of normal muscles and tumors were measured. The tumor-to-muscle (T/M) ratios of F-MISO SUV<sub>max</sub> were also calculated. Mean SUV<sub>max</sub> ± standard deviation (SD) of normal muscles was  $1.25 \pm 0.17$ , and SUV<sub>max</sub> above the mean + 2 SD ( $\geq 1.60$  SUV) was regarded as a hypoxic area. Nine of the 10 tumors had an F-MISO SUV<sub>max</sub> of  $\geq 1.60$ . All eight tumors examined twice showed a decrease in the SUV<sub>max</sub>, T/M ratio, or percentage of hypoxic volume (F-MISO  $\geq 1.60$ ) at approximately 20 Gy, indicating reoxygenation. In conclusion, accumulation of F-MISO of  $\geq 1.60$  SUV was regarded as an intratumoral hypoxic area in our F-MISO PET/CT system. Most human tumors (90%) in this small series had hypoxic areas before RT, although hypoxic volume was minimal (0.0–0.3%) for four of the 10 tumors. In addition, reoxygenation was observed in most tumors at two weeks of fractionated RT.

**Keywords:** tumor hypoxia;  $^{18}\text{F}$ -misonidazole; PET/CT; reoxygenation

## INTRODUCTION

Hypoxic cells of malignant tumors are considered to be radioresistant, and have been regarded as a poor prognostic factor in various cancers [1]. Misonidazole was found to be a hypoxic radiosensitizer by Asquith *et al.* in 1974 [2].  $^{18}\text{F}$ -fluoromisonidazole (F-MISO) was suggested as a tracer to determine hypoxic cells *in vitro* in 1983 [3]. To depict hypoxic lesions in human tumors, many clinical studies using F-MISO Positron Emission Tomography (PET) have been reported since 1991 [4]. In an animal experiment,

F-MISO image intensities were inversely correlated with measured intratumoral  $\text{pO}_2$  [5].

Over the past 10 years, use of PET/computed tomography (CT) has grown. PET/CT provides relevant information in the staging and therapy monitoring of many tumors because it can give more accurate identification of the anatomical site than PET alone [6]. All F-MISO studies reported before the early 2000s used PET alone instead of PET/CT. For radiation therapy (RT) treatment planning, PET/CT simulation has been used clinically [7], and hypoxic imaging obtained by F-MISO PET/CT may add

some useful information. Although many investigators used the tumor-blood (T/B) ratio, tumor-cerebellum (T/C) ratio, or tumor-to-muscle (T/M) ratio to evaluate intratumoral hypoxia using F-MISO PET with cut-off points of 1.2–1.4 [8–10], no study showed a hypoxic area threshold as an absolute value of F-MISO standardized uptake values (SUV). In the present study, 10 initial patients with various tumors were analyzed to determine a threshold value of SUVmax of F-MISO PET for intratumoral hypoxic areas, and to visualize their reoxygenation during fractionated RT in various human tumors. Also, the appropriate timing of F-MISO PET imaging after F-MISO injection was determined.

## MATERIALS AND METHODS

### Patients

Between November 2009 and April 2011, 10 patients scheduled for RT for primary or recurrent tumors were enrolled in this prospective study. Eligible patients had histologically proven malignant tumors, with a performance status (PS) level of 0–1 and were aged 20–80 years. Patients without gross target volume, pregnant or lactating women, and patients with mental disorders or severe organ disorders were excluded. Patient and tumor characteristics are summarized in Table 1. Ten patients, consisting of four with head and neck cancers, four with gastrointestinal cancers, one with non-small-cell lung cancer, and one with uterine body cancer, were included. The initial tumor response for both primary tumors and metastatic lymph nodes was evaluated by CT, magnetic resonance imaging (MRI), and clinical examination 1–2 months after the end of treatment according to the RECIST criteria (version 1.1) [11]. Because some tumors regress slowly, tumor response was evaluated at the maximum tumor regression between 1 and 2 months of treatment.

The study protocol was approved by the ethical committee of the Kinki University Faculty of Medicine. All patients signed informed consent before entering the study.

### F-MISO and $^{18}\text{F}$ -fluoro-2-deoxyglucose PET/CT protocol

Each patient was scanned with an integrated PET/CT unit (Biograph/Somatom Emotion Duo, Siemens Medical Solutions, Hoffmann Estates, IL, USA). All PET images were acquired using a matrix of  $128 \times 128$  pixels. The time for one bed position (162 mm in *z*-direction) scan was 120–150 sec. At a distance of 10 cm from the center of the field of view (FOV), the full-width at half maximum (FWHM) reached  $7.4 \text{ mm} \times 7.4 \text{ mm} \times 7.1 \text{ mm}$ , in the *x*, *y* and *z* directions, respectively. Voxel dimensions were  $4.5 \text{ mm} \times 4.5 \text{ mm} \times 2.0 \text{ mm}$ . CT scans were acquired in the spiral mode, with a slice thickness of 2–5 mm, a pitch of 6 mm, 130 kv and 55 mAs. The translation speed of the couch was 7.4 mm/sec. As a protocol, F-MISO PET/CT was performed twice before RT and during fractionated RT of ~20 Gy/10 fractions. Patients were injected intravenously with 7.4 MBq/kg of F-MISO. No fasting period before F-MISO injection was required. PET/CT was obtained twice, at 100 and 180 min after injection of F-MISO.

F-MISO was synthesized as described previously [12]. In short, in an automated synthesizer (F121, Sumitomo Heavy Industries, Ltd Tokyo, Japan), 5 mg of the precursor 1-(2'-nitro-1'imidazolyl)-2-O-tetrahydropyranyl-3-O-syl-propanediol (NITTP, ABX, Montpellier, France) in 0.3 ml of acetonitrile was reacted with a mixture of dried  $^{18}\text{F}$ -fluoride, 7.5 mg of Kryptofix 222 (Merck, Whitehouse Station, NJ, USA), and 2.77 mg of  $\text{K}_2\text{CO}_3$  at  $110^\circ\text{C}$  for 10 min. After hydrolysis with 0.3 ml of 1N HCl at  $80^\circ\text{C}$  for 10 min, 0.6 ml of 1N sodium acetate was added for

**Table 1.** Patients and tumor characteristics

No.	Age/Sex	PS	Primary site	Stage/Histology	Tumor length	RT dose	Chemotherapy
1	75/M	1	Maxilla sinus	T4a N1 M0/Sq	65 mm	42Gy/21fr <sup>a</sup>	CDDP, 5-FU
2	72/M	0	Esophagus	T3 N1 M0/Sq	30 mm	60Gy/30fr	CDDP, 5-FU
3	60/F	0	Uterine body	recurrence/Ad	48 mm	64.4Gy/35fr	none
4	46/M	0	Nasopharynx	T3 N2c M0/Sq	35 mm	70Gy/35fr	CDDP
5	57/M	0	Lung	T4 N3 M0/Sq	68 mm	60Gy/30fr	Nimotuzumab, CDDP, VNR
6	73/M	0	Esophagus	T3 N2 M0/Sq	28 mm	50Gy/25fr <sup>b</sup>	CDDP, 5-FU
7	72/F	0	Anal canal	T2 N0 M0/Sq	45 mm	59.4Gy/33fr	5-FU, MMC
8	72/M	0	Nasopharynx	T1 N2b M0/Sq	16 mm	70Gy/35fr	CDDP
9	56/M	1	Anal canal	T4 N1 M0/Ad	45 mm	45Gy/25fr <sup>b</sup>	5-FU, MMC
10	36/M	1	Nasopharynx	T4 N1 M0/Sq	42 mm	70Gy/35fr	CDDP

<sup>a</sup>RT was terminated due to severe acute toxicities. <sup>b</sup>Preoperative chemoradiation therapy. Ad = adenocarcinoma, CDDP = cisplatin, 5-FU = fluorouracil, MMC = mitomycin C, Sq = squamous cell carcinoma, VNR = vinorelbine.

neutralization. The product was purified with HPLC chromatography (YMC PAK ODS-AM 10 mm ID × 250 mm, YMC Co., Ltd, Kyoto, Japan) using 3:97 ethanol:H<sub>2</sub>O, and a 5.0 ml/min flow rate.

For all patients, <sup>18</sup>F-fluoro-2-deoxyglucose (FDG) PET/CT was performed before RT. The details of FDG PET/CT at our hospital have been described elsewhere [7].

### Radiation therapy and chemotherapy

For all patients, F-MISO PET/CT was performed before the start of RT, but this information was not used for the treatment planning. Eight patients were treated as definitive RT with a planned total dose of 60–70 Gy/30–35 fractions, although one patient terminated RT at 42 Gy due to acute renal failure caused by chemotherapy. The remaining two patients with gastrointestinal cancer were treated with pre-operative chemo-RT (CRT) in 45–50 Gy/25 fractions, and curative resection could be done following CRT for these patients. All patients except for a patient with recurrence of uterine body cancer were treated with concurrent chemotherapy. Details of the chemotherapy are summarized in Table 1. During RT, 2–3 cycles of chemotherapy were given.

### Analysis

Because normal tissues are considered to be under normoxia, F-MISO SUVs of normal muscles were measured. Data were processed with a Siemens e.soft workstation to measure SUV and hypoxic volume. In placing the volumetric regions of interest (VOIs) over the tumor and normal muscle, the SUVmax of the VOI on PET images was

adjusted by referring to CT images and PET/CT fusion images. SUVmax in 108 normal muscle areas was measured for all 18 F-MISO studies. For each study, six oval VOIs of 10–20 cm<sup>3</sup> were measured on bilateral posterior neck muscles (multifidus muscles, semispinalis capitis muscle, and semispinalis cervicis muscle), bilateral back muscles (erector spinae muscle, rhomboid major muscle, and trapezius muscle), or bilateral buttock muscles (gluteus maximus muscle).

For each study, F-MISO SUVmax values of both primary tumors and metastatic lymph nodes of >2cm were measured, and the highest value was regarded as the SUVmax of the study. To calculate the T/M ratio for head and neck tumors, thoracic tumors, or pelvic tumors, the average SUVmax of bilateral posterior neck muscles, back muscles, or buttock muscles was calculated, respectively. For statistical analysis, the paired Student's *t*-test was used to evaluate the difference between 100 min and 180 min after injection of F-MISO.

## RESULTS

Eight of the 10 patients underwent FMISO PET/CT twice: before RT and during fractionated RT. One patient refused a second F-MISO PET/CT due to the long examination time, and the other patient's second F-MISO PET/CT was cancelled due to acute renal failure caused by chemotherapy. Changes in SUVmax and the T/M ratio 100 and 180 min after injection of F-MISO in the pretreatment F-MISO study are shown in Table 2. Although large variations in F-MISO SUVmax in tumors were observed between 100 min

**Table 2.** Changes in SUVmax and T/M ratios at 100 and 180 minutes after injection of F-MISO in pretreatment F-MISO studies

No.	T/M ratio		SUVmax of tumor			
	100 min	180 min	100 min	180 min		
1	1.29	1.93	1.57	2.10		
2	2.66	2.66	2.79	3.06		
3	1.74	1.84	2.99	2.72		
4	1.88	1.86	2.25	2.06		
5	1.59	1.95	1.99	1.60		
6	1.65	2.38	2.33	3.12		
7	1.47	1.77	2.34	2.44		
8	1.22	1.08	1.43	1.35		
9	2.32	1.81	3.82	2.60		
10	1.56	1.61	1.75	1.71		
Tumor	1.74 ± 0.45 <sup>a</sup>	1.89 ± 0.42 <sup>a</sup>	NS	2.33 ± 0.72 <sup>a</sup>	2.28 ± 0.61 <sup>a</sup>	NS
Muscle				1.31 ± 0.24 <sup>b</sup>	1.25 ± 0.17 <sup>b</sup>	p = 0.01

<sup>a</sup>mean ± SD of the 10 tumors. <sup>b</sup>mean ± SD of 108 normal muscle areas.

and 180 min, the mean value of SUVmax was similar for 100 min and 180 min. On the other hand, the mean  $\pm$  SD of muscle SUVmax decreased significantly 180 min after injection compared to after 100 min ( $P=0.01$ ). Because of the decrease in the SUVmax of the muscle, the mean value of the T/M ratio at 180 min increased to 1.89 compared with the T/M ratio at 100 min. This means that F-MISO PET/CT images at 180 min had more contrast than those at 100 min. Therefore, we used F-MISO PET/CT imaging 180 minutes after the injection in the present analysis.

To determine the threshold of a hypoxic region, the SUVmax of the 108 areas of normal muscle were measured. The mean  $\pm$  SD of SUVmax for normal muscle 180 min after F-MISO injection was  $1.25 \pm 0.17$ . As the value of the mean +2 SD was 1.59 SUV, accumulation of F-MISO  $\geq 1.60$  was regarded as indicating a hypoxic area. Except for one nasopharyngeal tumor (Fig. 1), nine tumors had F-MISO SUVmax values of  $\geq 1.60$  prior to RT, indicating that these tumors contained hypoxic areas before treatment. To obtain high-contrast images and to depict hypoxic areas clearly, the window of F-MISO accumulation was set between 1.6 and 2.0 SUV. In addition, hypoxic volume (HV) was calculated (Table 3). HV was defined as the percentage of hypoxic volume (F-MISO  $\geq 1.60$ ) of the primary

tumor or metastatic tumor volume. HV was minimal (0.0–0.3%) for four of the 10 tumors (Table 3). For a patient with nasopharyngeal cancer, no F-MISO accumulation was observed either in the primary tumor or metastatic lymph nodes, although strong FDG uptake was noted (Fig. 1). There was no significant correlation between SUVmax of F-MISO and SUVmax of FDG accumulation for the 10 patients ( $r^2=0.037$ ).

Reoxygenation of tumors was evaluated in eight tumors on which F-MISO PET/CT studies were performed twice. Six of the eight tumors showed a decrease in SUVmax and/or the T/M ratio at approximately 20 Gy (Fig. 2). The remaining two tumors with increased SUVmax (cases 3 and 9) showed a decrease in HV, while one tumor with decreased SUVmax showed an increase in HV (case 6) (Table 3). Thus, all eight tumors showed a decrease in SUVmax, the T/M ratio, or HV, indicating reoxygenation. Figure 3 shows F-MISO PET/CT of a patient with anal canal squamous cell carcinoma (case 7). In this patient, both SUVmax and HV decreased in the second F-MISO study with 18 Gy/10 fractions.

The results of F-MISO studies and the initial tumor response of the 10 patients are shown in Table 3. In cases 2, 3, 6 and 9, SUVmax of the second F-MISO PET/CT still exceeded 2.5. None of the four tumors showed complete response (CR). On the other hand, four tumors with SUVmax of  $<2.5$  at the second F-MISO PET/CT showed CR or partial response (PR) with long term local control (case 5). Similarly, all four tumors with HV of  $<6.0\%$  in the second F-MISO study showed CR or PR with long-term local control.

## DISCUSSION

In the present study, the threshold of F-MISO PET for hypoxia was determined as an absolute value of F-MISO SUV. Most previous reports used the T/M ratio or T/B ratio in the definition of tumor hypoxia [8–10]. To introduce F-MISO images to RT planning, a threshold of hypoxia as an absolute value of F-MISO SUV is easy to use. In addition, absolute values of F-MISO SUV can be translated to partial pressure for oxygen ( $pO_2$ ) based on an experimental study [13]. Another advantage of using absolute values of tumor F-MISO SUV is to eliminate errors in measurements of SUV for normal tissues. We measured the absolute values of F-MISO SUV for many muscle points to determine the range of F-MISO SUV of normal muscles. PET alone has limited spatial resolution compared with PET/CT. Therefore, the PET/CT used in the present study could measure the SUVmax of many areas of normoxic muscle accurately. The threshold for hypoxia was determined to be SUV of F-MISO equal to 1.60 because the mean SUVmax +2 SD of muscles was 1.59. The range of SUVmax in tumors in this study was 1.35–3.12 with a

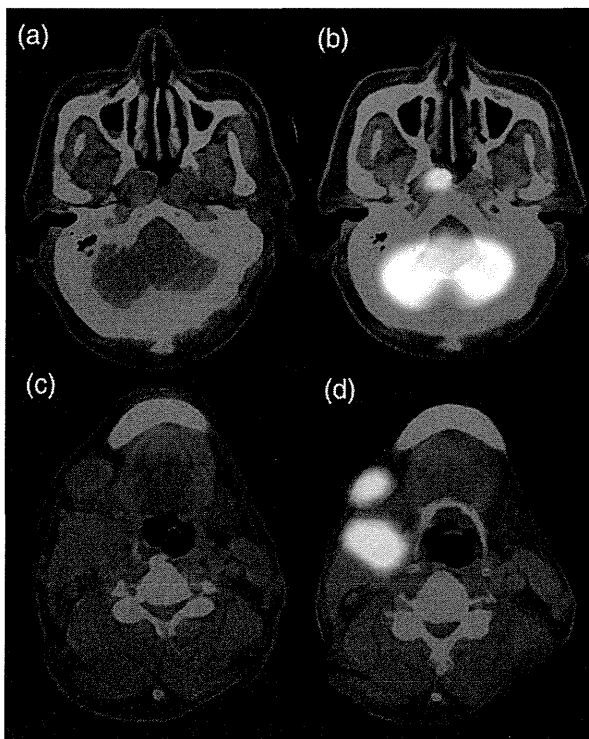


**Fig. 1.** F-MISO PET/CT (a, c), and FDG PET/CT (b, d) for a patient with nasopharyngeal cancer (case 8: T1N2bM0). In this patient, no significant F-MISO accumulation was observed in the primary tumor (SUVmax; 1.20) or metastatic lymph nodes (1.35), although strong FDG uptake was noted.

**Table 3.** Changes in F-MISO SUVmax and hypoxic volume (HV) and the initial tumor response

No.	Disease	Treatment	1st-FMISO		2nd-FMISO		Tumor Response
			SUVmax	HV(%)	SUVmax	HV(%)	
1	Maxillary ca.	CRT: 42Gy/21fr	2.10	2.7			PD
2	Esophageal ca.	CRT: 60Gy/30fr	3.06	75.6	2.50	24.6	PR
3	Uterine body ca.	RT: 64.4Gy/35fr	2.72	42.3	3.32	36.5	PR
4	NPC	CRT: 70Gy/35fr	2.06	0.3	1.43	0.0	CR
5	Lung ca.	CRT: 60Gy/30fr	1.60	0.0	1.70	0.0	PR <sup>a</sup>
6	Esophageal ca.	CRT: 50Gy/25fr	3.12	6.7	2.69	7.9	NC
7	Anal canal ca.	CRT: 59.4Gy/33fr	2.44	7.6	.08	2.2	CR
8	NPC	CRT: 70Gy/35fr	1.35	0.0			CR
9	Anal canal ca.	CRT: 45Gy/25fr	2.60	65.8	3.16	6.1	PR
10	NPC	CRT: 70Gy/35fr	1.71	0.1	1.32	0.0	CR

<sup>a</sup>Although the tumor response evaluated by the RECIST criteria was PR, local control was achieved for >2 years.

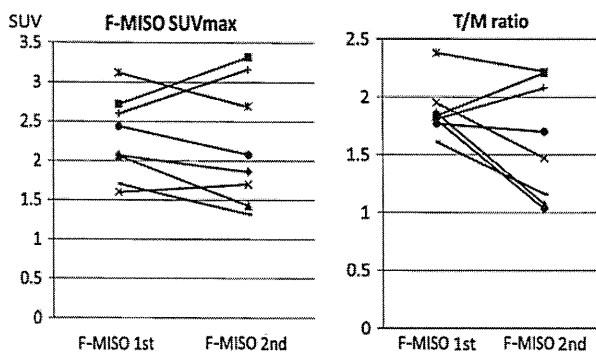


**Fig. 2.** Changes in F-MISO SUVmax and T/M ratios for eight patients. Six of the eight tumors showed a decrease in SUVmax and/or the T/M ratio after approximately 20 Gy of fractionated RT.

median of 2.1, which is similar to other previous reports [14, 15].

SUVmax of muscles decreased significantly at 180 min after injection of F-MISO compared with that at 100 min. This may be attributable to the fact that F-MISO in tumor hypoxic areas exhibits slow clearance due to its high lipophilicity. Because of the difference in accumulation and clearance of F-MISO between tumors and normal tissues, it has been reported that the T/M ratio increased up to 3 h after injection of F-MISO [10, 16]. This means that F-MISO PET/CT images at 180 min had more contrast than those at 100 min. Therefore, we used F-MISO PET/CT imaging 180 min after the injection in the present analysis.

In terms of oxygen tension in F-MISO-accumulated areas, one animal experiment using a pig liver showed that F-MISO preferentially binds when  $pO_2$  is < 15 mmHg [13]. In that study, the F-MISO SUV of 1.57 corresponded to a  $pO_2$  of 20 mmHg. Therefore, F-MISO-accumulated areas

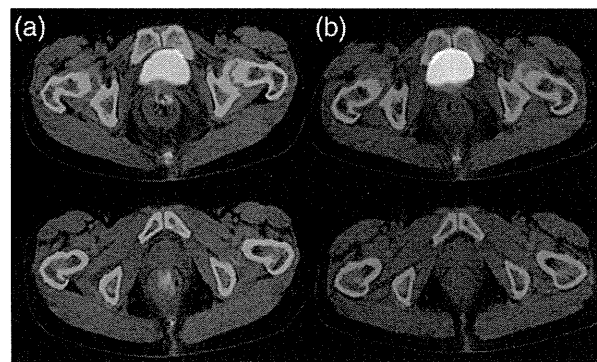


**Fig. 3.** F-MISO PET/CT (a) before RT, and (b) during RT (18 Gy/10 fractions), for a patient with anal canal squamous cell carcinoma (case 7: T2N0M0). In this patient, F-MISO accumulation in the primary tumor (SUVmax; 2.44) decreased to 2.08 in the second F-MISO study at 18 Gy/10 fractions.

with a threshold of 1.6 SUV in the present study may represent hypoxic areas with a  $pO_2$  of <20 mmHg. The oxygen enhancement ratio (OER) was approximately 3 under well-oxygenated conditions and it decreased for  $pO_2$  below 20 mmHg [17]. The OER decreased to 2.0–2.8 at an oxygen tension of 3–20 mmHg. Thus, the F-MISO-accumulated areas are radioresistant compared with other normoxic regions.

In the present study, SUVmax, the T/M ratio, or HV decreased in all eight tumors after approximately 20 Gy, indicating reoxygenation. It is reported that errors in measurements on SUVmax are approximately 10%, so a decrease in SUVmax of > 10% may be significant [18, 19]. Except for case 5, the decrease in SUVmax was > 10% for the eight tumors (Table 3). Notably, for case 9, SUVmax increased in the second F-MISO study (Table 3), although HV decreased to 6% from the initial value of 66%. HV may be a more appropriate indicator for reoxygenation than